Chapter 6

Electrophysiological Characterization of Dopaminergic Neurons of the Rat Substantia Nigra Compacta

Marcelo Aguilar-Rivera, Rafael Ignacio Gatica, Victor Azócar, Darinka Buc, and José Antonio Fuentealba-Evans

Abstract

Dopamine neurons of the substantia nigra pars compacta (SNc) are involved in several physiological and pathological processes, ranging from motor control to decision-making. For example, a deficit in the activity of these neurons is associated with Parkinson's disease, while an increase in their activity has been associated with the compulsive drug seeking. Therefore, the study of the electrical activity of the SNc neurons is essential to continue studying the contribution of the nigrostriatal pathway to cognitive and behavioral processes. In this chapter, we describe a detailed protocol to carry out electrophysiological "single-unit recording" in dopamine neurons of the SNc in anesthetized rats. In addition, we provide electrophysiological criteria to classify different neuronal types and statistical tools to determine the effect of an acute injection of amphetamine on the activity of SNc neurons.

Key words Dopamine, Substantia nigra, Single cells, Tetrodes, Action potential, Firing rate, Firing pattern, Amphetamine

1 Introduction

Evidence suggests that dopaminergic neurotransmission is among the most important factors adjusting behavioral control [1]. Dysfunction in dopamine signaling has been associated with disorders sharing failure in behavioral control, such as drug addiction, attention-deficit/hyperactivity disorder, and obsessive-compulsive disorder [2, 3]. Two involved dopaminergic pathways have been described: the mesolimbic dopaminergic pathway that comprises dopamine (DA) neurons from the ventral tegmental area (VTA) to the nucleus accumbens (NAc) [4] and the nigrostriatal pathway involving DA neurons from the substantia nigra compacta (SNc) to the dorsal striatum [5, 6]. In this regard, electrophysiological recording in anesthetized rats show that the repeated exposure to drugs of abuse is accompanied by an increase in firing rate and burst

José Antonio Fuentealba-Evans and Pablo Henny (eds.), *Dopaminergic System Function and Dysfunction: Experimental Approaches*, Neuromethods, vol. 193, https://doi.org/10.1007/978-1-0716-2799-0_6,

activity in DA neurons of SNc and VTA [7, 8]. Thus, the objective of this chapter is to describe a protocol to carry out electrophysiological recordings of DA neurons in the SNc.

There has been a notorious evolution in the type of electrodes used to record cell units and field potentials in the alive brain: from single wire electrodes, made of different metal alloys that started being used early in the last century, to high channel density silicon probes widely used nowadays [9]. The electrophysiology recording technique is continually being improved not only to record more cell units from multiple sites but also to get a better fidelity of the recorded neural signal. Both low channels and high-density recordings have advantages and disadvantages regarding electrode hardness vs brain damage, or impedance vs noise, and price vs usability, so the trade-off should be evaluated in virtue of the biological questions under research. For instance, in some cases inexpensive wire-based electrodes are good enough to explore correlational hypothesis about brain activity on anesthetized preparations where live brain tissue is recorded only once. However, other metal alloys such as platinum iridium (PtIr) are more convenient to explore a causal hypothesis that involves the manipulation of neural activity, for instance, by electric stimulation [10] through the same electrodes used to record action potentials. The recording of brain activity at the single cell level and from multiple sites is challenging since it involves the use of small manipulators to control single or multiple electrode bundles with the help of a mechanical system named microdrive. Such microdrive as that presented in this chapter allows us to control the electrode depth into the brain tissue. Importantly, a microdrive can be configurated to target more than one brain area, using for simplicity, a single bundle array. In this case, the tip of each tetrode or some tetrodes subsets can record at different depths into the brain due to different wire length. In this way, the same bundle will be composed by two subsets of electrodes where the only difference between subsets is the tetrode length. In this chapter, the main aim is to discuss affordable electrophysiological approaches to study DA neurons of SNc in anesthetized animals.

2 Materials and Drive Components

Before starting to build a microdrive, it is necessary to define the tetrode configuration associated with the biological research questions to be researched and the target brain areas to be recorded. In this regard, it is necessary to define the rostral-caudal, medial-lateral, and dorso-ventral stereotaxic coordinates using an atlas such as the Paxinos and Watson atlas [11] or the Swanson's brain atlas [12]. Both atlases are specific for rat strains and a weight of 290 g, so to increase the targeting precision, the stereotaxic coordinates should follow such weight.

Usually, single tetrode arrays with a specific spatial configuration, for instance, 4 columns by 2 rows, with a total of 8 tetrodes (32 channels), are easy to build and will be optimum for targeting most of the brain areas, including those associated with the mesolimbic and nigrostriatal dopaminergic pathways. However, it is always possible to create more customized tetrode arrays, with different and specific spatial configurations, depending on the hypothesis under consideration and the skills of the researchers building such arrays.

We present a step-by-step guide to build tetrodes, tetrode arrays, and microdrives that allow for the control of tetrode positioning on the dorsal ventral axis. Also, we discussed some of the most standard analytics to quantify changes in the firing rate as well as how to qualitatively measure the way that dopaminergic neurons fire action potentials.

In a general sense, five different steps can be identified from wires selection to manipulator assembly as discussed below. In short, we refer to these steps as (1) selecting wires, (2) assembling manipulator, (3) soldering the tubing array, (4) twisting tetrodes, and (5) electrode interfacing using a printed circuit board (PCB).

A list of materials that includes the type of material and preferred sellers are listed in Table 1. Figures 1, 2, 3, 4, 5, and 6 present the most standard techniques and analysis in neuroscience to record neural activity and then study firing rate patterns in a quantitative way.

2.1 Wire Selection

There is a well-known relationship between the metal alloy of which a wire is made and its softness or stiffness. Stiff wires such as tungsten could be preferred to target deep brain areas as they can succeed in reaching all the way down (~8 mm) to the deepest tissue, for instance, when recording DA neurons from the VTA [13, 14]. Here we presented an alternative option based on cheaper wires, such as NiCr, that attain good enough stiffness based on twisting to successfully reaching deep brain area such as the SNc, when these types of wires are tied and twisted together.

Additionally, there are other electrode features such as the inverse relationship between area and impedance of an electrode that could also determine the recording quality. Electrode impedance is one of the most relevant features as described in the classic electrophysiological literature [15], as well as in a comprehensive discussion on this topic by Roger Lemon in 1984 on his book *Methods for Neuronal Recording in Conscious Animal* [16]. On the Chapter 5 entitled "Microelectrodes and Microdrives," Roger discussed the electrical and biological properties of microelectrodes based on the detailed previous work of David Robinson [15]. Both readings, highly recommended, describe different electronic and biological parameters such as impedance, capacitance, and the resistance associated with the brain–electrode interface, as well as

Table 1
Materials and reagents for tetrode electrodes and manipulator

Material	Company	Contact
Micromanipulator		www.nervetools.com
PCB		www.nervetools.com
Stainless steel tubing, 27G, 0.016″ OD, 0.002″ wall, 0.012″ ID (guiding cannulae array)	MicroGroup	https://microgroup.com/
Stainless steel tubing, 32G, 0.009″ OD, 0.002″ wall, 0.004″ ID (thinnest cannula to protect each tetrode)	MicroGroup	https://microgroup.com/
18-8 Stainless steel machine screw, plain finish, pan head, slotted drive, 1/8 length, fully threaded, 0-80 threads	Amazon, Grainger, McMaster-Carr	www.amazon.com www.grainger.com/ www.mcmaster.com/
Tetrode wire 0.0005″ (tetrode wire)	Sandvik Co.	https://www.materials.sandvik/en/
Small gold pins	Neuralynx	https://neuralynx.com/
36 position dual male nano-miniature connector A79022-001	Omnetics Connector Co.	https://www.omnetics.com/
PFA-coated stainless steel wire, 0.003″ bare, 0.0055″ coated (ground wire)	A-M Systems	https://www.a-msystems.com/
Gold plating solution	Neuralynx	https://neuralynx.com/

The main components are stainless steel and 3D printed plastic materials. There are several vendors around the globe from where to buy such materials and also some open sources from where to download, for instance, the 3D files for the manipulators. Depending on the type of neural potentials and brain areas, some materials are preferred for electrode twisting (i.e., stereotrodes and tetrodes), as discussed in the main section

the metal's electrode alloy, length, electric insulation, and shape of specific wires that determine the impedance and therefore the signal-to-noise ratio of electrophysiological recordings. In summary, the surface area, mostly related to the diameter of the exposed tip of an insulated wire, and its associated impedance are two key features to take into consideration on the fabrication of custom-made electrode array. Such features determine the noise and the fidelity of the neural recordings, and they can have a specific impact on the recording of single units and field potentials.

Using a thick wire, between 50 and 100 μm, is preferred to record field potentials since the thicker the wire the more cell

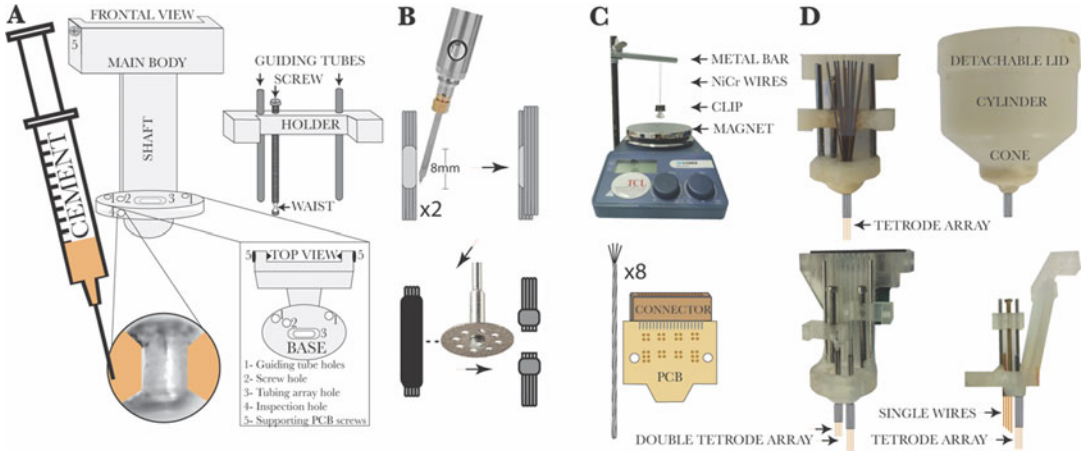

Fig. 1 Assembly of single and multiple electrode arrays. (**a**) 3D plastic parts that allow to hold vertically the printed board circuit and to control the electrode array positioning in the vertical axis. The drive is a simple mechanism based on a modified 00-80 stainless steel screw as discussed in the main text, two 21G cannulae glued to the base by any cyanoacrylate, and a horizontal plastic holder. To fill the space around the waist screw with dental cement, it is possible to use a 1-mL syringe and a thick needle (18 or 19G). (**b**) Assembly of stainless steel 27G cannulae array to spatially organize electrodes (i.e., 4 × 2 tetrodes) and guide them down into the brain. With the help of a soldering iron, eight cannulae are soldered (4 × 2 cannulae) side by side using tin (gray area). Then the array is cut in half to get two cannulae arrays. For this, the cannulae array is protected by a shrink tube (black area), thus preserving the recently soldered cannulae array. (**c**) Tetrode twisting process showing how to hang two wires from a horizontal bar placed over a magnetic dish. After bending the pair of wires around the bar, a loop is formed having four wires that will be twisted together to form a tetrode. Also, the custom PCB is depicted. (**d**) Different examples of the electrodes array configuration. Top panels depicted the eight tetrode arrays used in our recordings from the SNc (as in Figs. 3, 4, 5, and 6). The bottom panels show two other examples of tetrode configurations to target multiple brain areas. At the left two bundles of four tetrodes each, one to reach the amygdala and the other for the insular cortex. At the right, a multiple electrode array is optimized to record action potentials using thin tetrodes (12 μm) and field potentials using thicker (~100 μm of diameter) single wires

activity can be recorded. This allows for a good proxy of the averaged brain activity of hundreds to thousands of neurons [17] around the electrode tip. On the other hand, the use of thin wires optimizes the recording of action potentials from single cells since tiny wires can get closer than thicker wires to the neural bodies. An electrode with a small tip area will record changes on the membrane potential over a smaller distance than an electrode with a course tip, increasing the selectivity of such a thin electrode and the chance to well isolate action potentials sourced by single neurons. This proximity involves a small electric distance between the wire tip and the cell body or axon, increasing the spatial resolution that favors the recording of well-defined waveforms whose peak amplitude is "away" (usually >2 standard deviations) from the averaged background noise. Thus, the use of thin wires optimizes the spike sorting that is a common analytic based on the neural waveform as described later in this chapter (Fig. 3). However, a potential

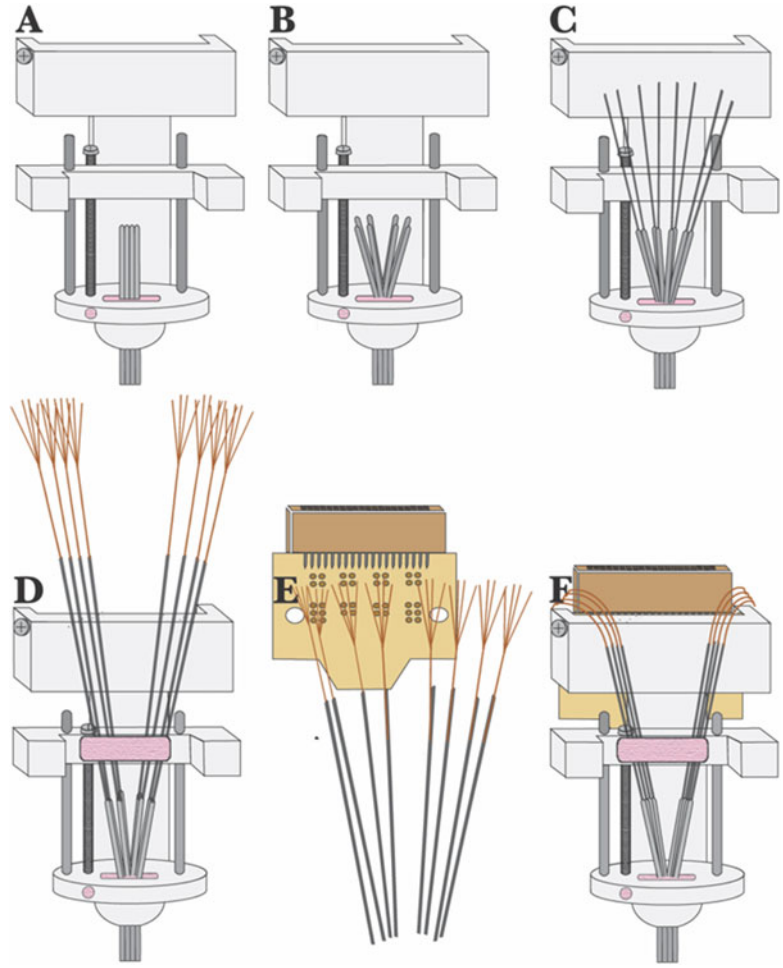

Fig. 2 Step-by-step assembly of a custom single electrode array. (**a**, **b**) The modified screw and cannulae are installed in the plastic base of the manipulator. Since the screw is trapped to the base by dental acrylic around the waist, it can spin on its own axes, and only the horizontal plastic part moves up or down. The guiding cannulae array also is installed in the base. The tip of the cannulae array should protrude ~6 mm from the bottom end of a manipulator to see under the manipulator and over the brain (i.e., during cutting the dura), for instance, when recording under anesthesia or during implantation of a manipulator for chronic recordings. The tetrode length has to stay in the case and should be able to protrude up to approximately 9 mm from the tip of the cannulae array to reach deep brain areas as the dopaminergic neural tissue. (**c**) The thinnest cannulae (32G) should be installed inside of the 27G cannulae array. (**d**) Next, each tetrode is installed one by one inside the thinnest 32G cannulae. The horizontal holder has to be in the upper position, so the tetrode can move all the way down, ~9 mm here, after tetrode is glued to the holder. For this, glue each tetrode to each 32G cannula using loctite, as well as cement the 32G cannulae using dental cement to the horizontal plastic holder (pink area). (**e**) The PCB is placed vertically behind the main plastic part, and each wire of a tetrode is interfaced to it using a gold pin. For simplicity, the main body and microdrive are not shown on the draw at the right. (**f**) The PCB is kept in place by lateral screws, but in addition, it can be secured to the connector holder by a small amount of dental cement

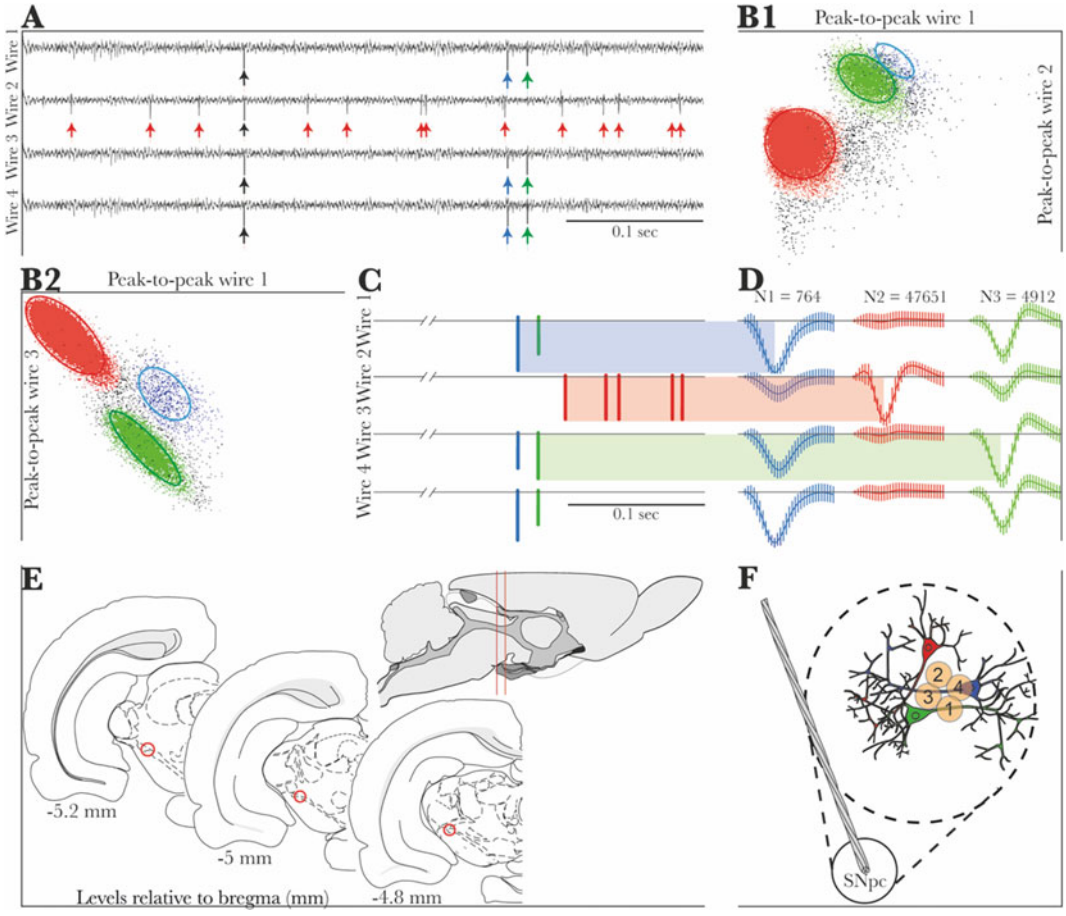

Fig. 3 Example of a canonical tetrode recording and spike sorting of single neurons. (**a**) Four traces depict a raw recording of high-frequency (300–5000 Hz) electrical neural activity from each wire of a tetrode. The multiple color arrowheads show three potential single neurons, while black arrows depict a single noise event that appears with equal amplitude at the four channels simultaneously. (**b1**) Scatter plots of the peak-to-peak amplitude of the action potential waveforms recorded in wire 1 versus those recorded in wire 2, while **b2** depicted spike activity recorded by wire 1 vs wire 3. Both scatter plots depicted the amplitude waveforms from the SNc record shown in **a**. Two clusters clearly emerge in the first plot **b1**, while the third cluster in blue is not evident away and separated from the cluster in green. However, the scatter plot **b2** shows complementary information where clusters in red, green, and blue are not overlapped, disambiguating that the action potentials in clusters in blue come from a different neuron than the red and green clusters. This is confirmed with the averaged waveform depicted in **d**. (**c**) Pictorial representation of the sorted spike trains extracted from the traces shown in **a**. (**d**) The extracted spikes from the clusters shown in **b**. Shaded area connected to **c** represents the same spike. The neuron 1 (blue) is captured clearly by wires 1, 3, and 4. Neuron 2 (red) shows as a well-defined waveform in wire 2, while neuron 3 (green) is evident in wire 3 and also in wires 1 and 4. Vertical lines around the averaged waveform represent ± 1 standard deviation. (**e**) Pictorial representation of rat brain coronal cuts on the rostral-caudal axis (modified from [12]). Red circles bound the area where tetrodes were lowered. (**f**) Scheme that represents the electric distance from the three neurons to each wire of the tetrode analyzed in this figure. The amplitude differences on the averaged waveform showed in **d** can be understood as the distance of the four tetrode channels to the neurons around. Every time a cell fires, action potentials are recorded simultaneously by the four channels that are part of the tetrode

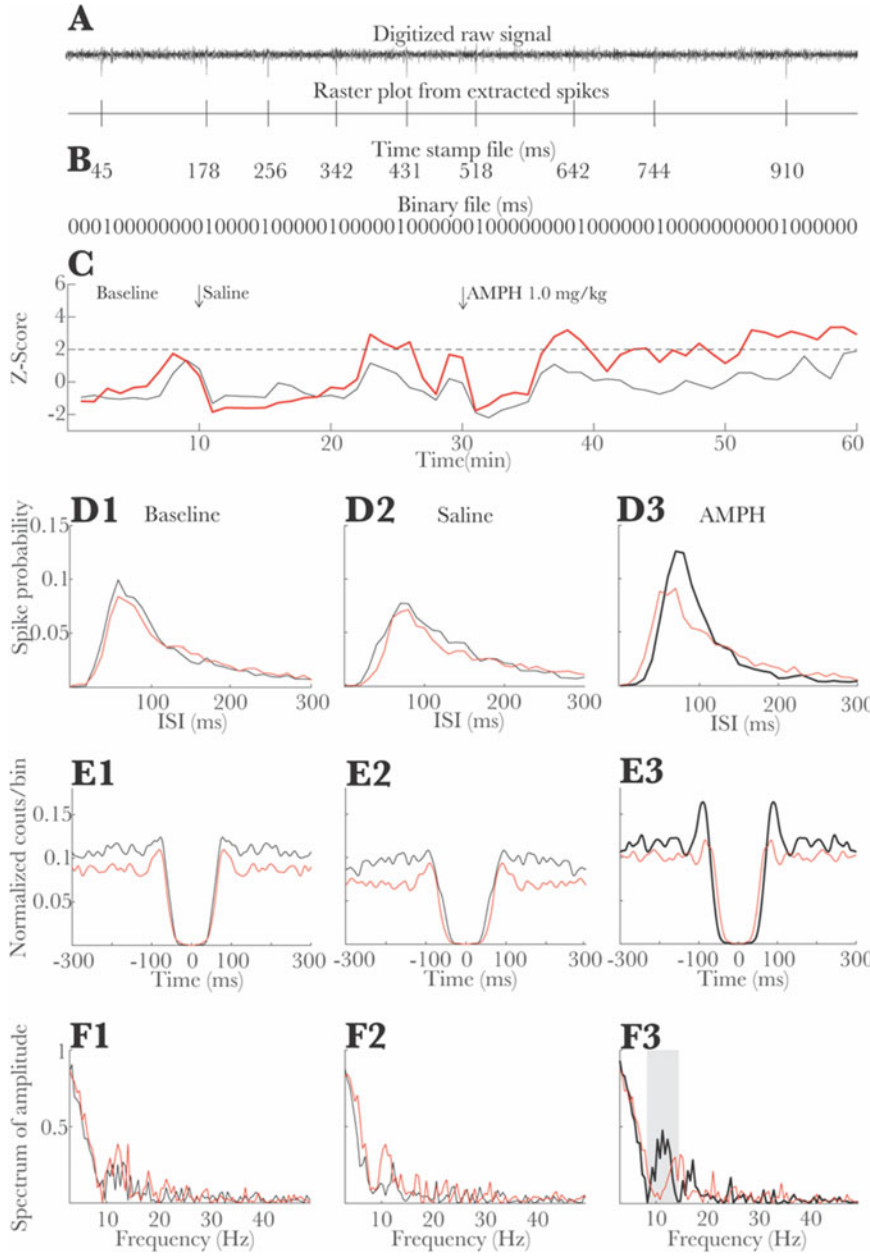

Fig. 4 Spikes extraction and firing rate characterization. (**a**) Top trace depicts a digitized raw signal of high-frequency (300–5000 Hz) neural activity as action potentials. It is possible to see the single spike events as a sharp vertical deflection. The bottom trace shows a raster plot of the extracted spike as a vertical line that matches temporally the single spikes events on top. (**b**) The top and bottom series are the timestamps and binary files, respectively, from the raster plot in **a**. (**c**) Changes on firing rate that are expressed as a *Z*-score from the baseline for a sequence of bins (60 s each bin) before and after injections. Red and black traces represent two different neurons. It is possible to observe a steady increment of the firing rate after AMPH 1.0 mg/kg ip that is significant (permutation test: $p < 0.05$) only for the neuron represented by the red trace. Interestingly, AMPH did not significantly change the firing rate on the second neuron (black trace). (**d**) Histograms of the interspike interval (ISI) during baseline, post-saline, and post-AMPH. The same number of spikes ($N = 3700$) was used to compute each histogram. It is possible to see that AMPH injection increased

drawback of thin wires (10–12 μm) is a high impedance (>2 MOhm) with a putative detriment of the quality signal since an increase of the noise. It is possible to reduce electrode impedance (even <1 MOhm) by metal deposition through gold plating, or by grinding the electrode tip [18], with the help of a diamond wheel spinned by a Dremel.

One of the low impedance reasonably priced wires on the market is the 50-μm tungsten wire (by California Fine Wire™). This wire is insulated with a single polyimide layer (SML) of coating around the tungsten metal bar. Given that polyimide has an excellent thermal stability, the heat treatment of such coating after twisting has a minimal effect on preserving the characteristic tetrode shape. Many researchers still prefer tungsten wires when the main goal is to record field potentials and spikes. Several wire alloys have been used to record both field and spikes activity from rats, although an ~65-μm diameter looks like the superior limit to successfully record action potentials and to get well-isolated waveforms [19].

Other researchers prefer to use alloys that are coated with materials that keep the shape of the twisted electrodes after activation by heat. One example is electrodes insulated with polyimide resin coating such as polyamic acid solution (PAC) as on the Sandvik™ wires. When this resin is exposed to heat, it helps to preserve the tetrode shape after twisting. Additionally, this type of coating reduces the biological response during chronic implants. Another option is to use a Heavy Formvar (HFV) with a secondary heat-activated bond coat from California Fine Wire™ and A-M systems™ that also helps to keep tetrodes twisted after treating the wire coating with heat. A nickel-chromium (NiCr) wire with such a heat-activated coating is a good combination since it retains the tetrode shape after twisting and activation by heat. Moreover, NiCr wires are cheaper than other alloys like tungsten or (platinum iridium) PlIr wires. Another benefit of using NiCr wires is the fact that is possible to find bars with diameter as thin as 10–12 μm, which is wanted to optimize single-cell recordings. We have gotten good quality recordings using NiCr alloy of 12 μm of diameter [20–22]. As discussed below, it is possible to get a good signal-to-noise ratio besides clearly identifying the waveforms from a single cell, where the functional concept of "unit" is further confirmed by functional measurements calculated from its firing such as the interspike interval (ISI).

Fig. 4 (continued) the chance that consecutive spikes are fired with a time delay under 100 ms for the neuron represented by the black trace. (**e**, **f**) Autocorrelograms and their respective power spectrums were calculated for the same neurons and periods of time as in **d**. This analysis confirms that amphetamine-induced change (gray shade area) on the firing mode only for the neuron represented by trace in black

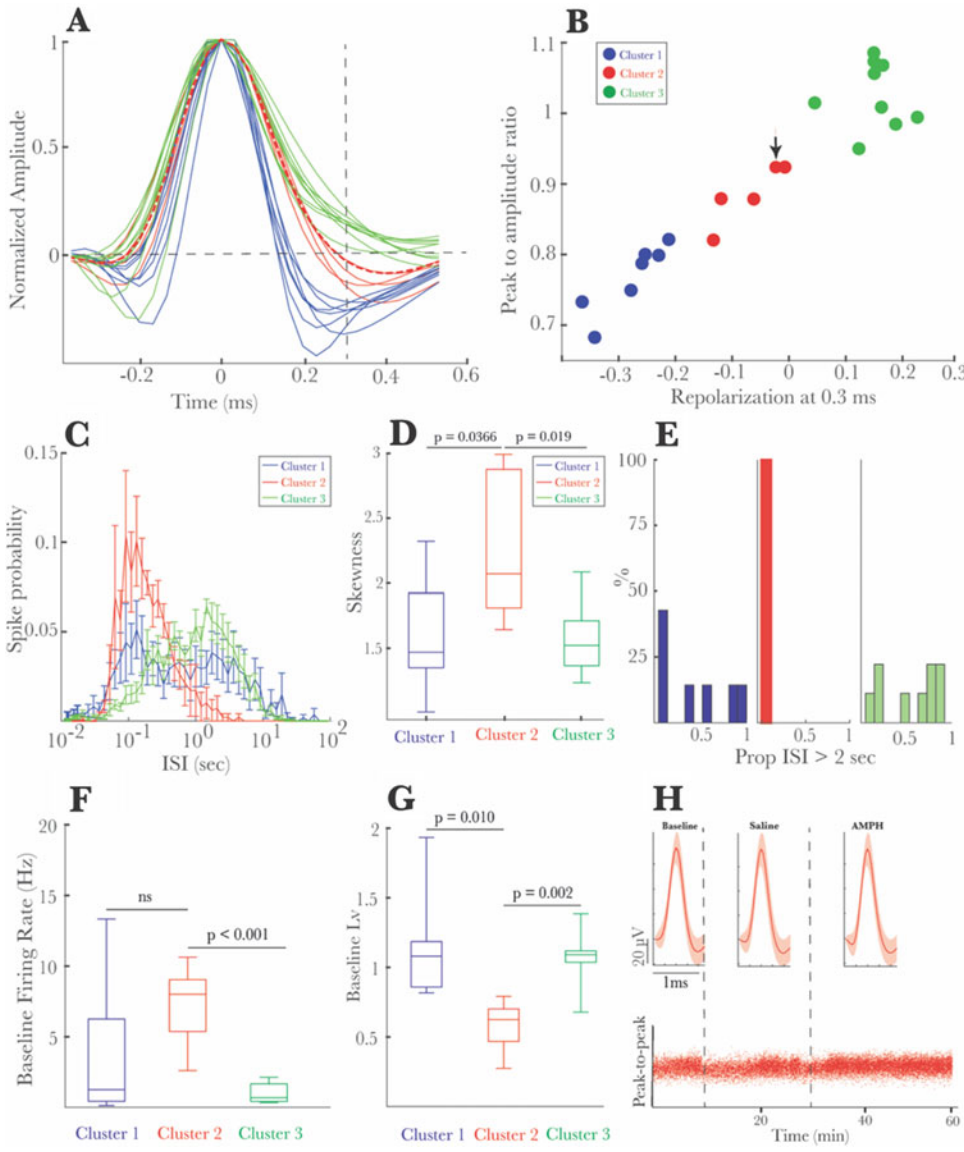

Fig. 5 Neural phenotypes classification based on waveform and spike firing. (**a**) Normalized waveforms of three different putative neural phenotypes. Since during repolarization waveform differs significantly among groups, the repolarization value at 300 us after the peak (dotted vertical line) was used for clustering as shown in the figures. (**b**) Scatter plot of repolarization values (as in **a**) versus the peak to amplitude ratio showing the separation of three neural phenotype clusters recorded from the SNc. The arrow in the second cluster in red depicts the neuron showed in **h**. (**c**, **d**) Averaged histograms of the interspike intervals (ISI) for the three phenotypes. It is possible to see that the cluster of putative dopaminergic neurons in red shows a distinctive distribution of ISI with a rise around 100 ms (10^{-1} s), having this a significant positive skewness as in **d**. The same number of spikes ($N = 200$) per neuron was used to compute each histogram before averaging them. This means there is a bigger probability these putative dopaminergic neurons fire action potentials with a short time among spikes ~100 ms (10^{-1} s). The chance that these putative dopaminergic neurons fire action potentials with a long time among spikes is low as depicted by the histogram in red of (**e**). (**f**, **g**) The cluster of putative dopaminergic neurons has a higher basal firing rate compared to cluster 3 and a smaller Lv than clusters 1 and 3 ($p < 0.05$, Mann-Whitney test). (**h**) Typical electrophysiological example showing a steady

When the aim is also to perturbate brain activity by electric microstimulation through the same electrodes used to record neural activity, platinum iridium (PlIr) alloy is a good option since it is less sensitive to the redox process associated with electric microstimulation than NiCr [23]. Additionally, this alloy has a lower impedance than NiCr and evokes minimal scarring in chronic implants [10], although PlIr alloy is an expensive type of wire.

2.2 Manipulator Assembly

The manipulator is a set of 3D printed plastic parts that contain and protect all its components, such as the tetrode array, the PCB, the microdrive, and the main body (Fig. 1). The microdrive is the main mechanical component of a manipulator that allows to move a tetrode array vertically, that is, dorsally and ventrally, into the brain in a very controlled way. This microdrive is composed of a modified screw, a couple of guide tubes, and a plastic horizontal holder where the tetrodes are glued (Fig. 1a). Next to the drive system, there is a shaft that serves as the physical support where the PCB is placed (Fig. 1a). The PCB is the physical interface between each wire of a tetrode (Fig. 1c) and the headstage amplifier. This printed circuit has 36 gold-plated vias where every one of them works as a channel (~330 μm in diameter) to insert one of the ends

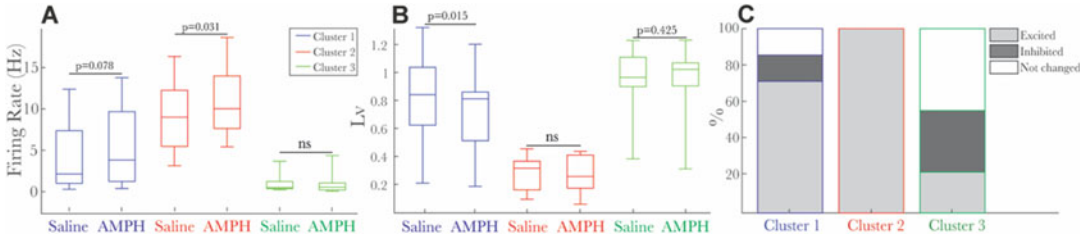

Fig. 6 Changes in the rate of action potentials on putative dopaminergic neurons induced by amphetamine injection. (**a**, **b**) Firing rate and Lv analysis. AMPH 1.0 mg/kg ip triggered a significant change in the number of spikes per second (**a**), but not on the firing pattern of putative dopaminergic neurons (**b**, depicted in red, $N = 6$). On the other hand, a decrease in irregular firing, without changes in firing rate, was found on non-dopaminergic neurons (depicted in blue, $N = 8$, Wilcoxon signed-rank test $p < 0.05$). Moreover, AMPH injection did not induce changes in firing rate or Lv of those non-dopaminergic neurons depicted in green. Data are represented as box and whiskers, showing the median (middle line), the 25th and 75th percentile in the box, and the lowest and highest values (whiskers). (**c**) AMPH population response analysis. After AMPH 1.0 mg/kg ip, neurons from clusters 1 (non-dopaminergic) and 2 (dopaminergic) were mainly excited, while both excitation and inhibition were mainly found in cluster 3 (non-dopaminergic). Data is shown as stacked bars

Fig. 5 (continued) waveform amplitude of action potential discharges of a neuron (pointed by the arrow in **b**) through the whole 1 h of recording. Based on the cloud density, it is possible to see an increment of firing rate after amphetamine injection. Boxplot depicts median and percentile 25th and 75th, while whisker depicted minimum and maximum

of every wire that is part of the tetrode. The other end of the same tetrode is inserted in the brain after opening the dura. Also, three of these vias are to interface the ground electrodes, and one via works as the interface for reference. This PCB has soldered a military-grade connector (by Omnetics) for 32 channels plus 3 grounds and 1 reference channel. This board allows to electronically interface the whole tetrode array placed in the brain and the ground usually placed on the skull, to a headstage pre-amplifier. The microdrive allows to control the tetrode positioning during acute recordings under anesthesia or several days after the implantation surgery when the animals are fully recovered from surgery. The microdrive is composed of two stainless steel guiding tubes (21G) that are glued to the main plastic body floor (Fig. 1a). If such tubes are not available in the laboratory, it is also possible to use the stainless steel portion of 21G needles after cutting the bevel portion and rounding both ends. Such a 21G tube vertically guides the sliding of the movable horizontal plastic holder where the electrodes are glued. The use of a modified screw, that has a waist in the lower portion of the shaft, is justified by the need to trap the screw, avoiding it to move up or down but still letting it spin on its own axis moving the electrode holder instead. The waist on the screw is made with the help of a Dremel, 1 mm upper from the bottom edge of the screw. This is a stainless steel narrow cheese head slotted 0–80 screw, and the waist is ~400-μm deep so the diameter is ~700 μm in the deepest portion of the waist, while the unmodified remaining thread portion is 1.5 mm of diameter. Pouring acrylic cement, for instance, using a 1-mL syringe and a thick needle, i.e., 18G, through the lateral inspection hole helps to trap the screw when the cement dries around the waist (Fig. 1a, frontal view). Thus, the screw can spin in a clock and counterclockwise, moving up or down, respectively, the horizontal plastic holder along with the tetrode array glued on it, to different deepness into the brain. During the screw planting and before the dental acrylic cure, the screw must be rotated penetrating a tinny oil machine drop. If it was correctly done, the screw will rotate without getting out of piece. The movement on the vertical axis of this system is equivalent to 312 μm for each full turn screw and 78 μm when the screw is spinned only a quarter of a full turn. In summary, the microdrive is a simple but critical component to move tetrodes.

2.3 Tube Array Soldering

To build an array of cannulae that guide the movement of electrodes down into the brain, eight stainless steel guide cannulae 27G of 4 cm length are needed. It is also possible to use the shaft of 27G long needles to prepare such array. Solder together the four cannulae side by side by spreading tin on the top surface and covering 8 mm distal on each side from the middle of the array. Repeat the process with the remaining four cannulae (Fig. 1b). The new two half must be soldered together using the other face that is free of

soldering (Fig. 1b). After soldering both halves together, you will have a single array of eight cannulae in total and organized as four by two cannulae. Before cutting the cannulae array in the half, it is necessary to cover the array using a heat shrink tube of 3 cm length. This will protect the array from damage when it is being cut in the middle to get the two halves of four by two cannulae (Fig. 1b). After cutting the array, it is necessary to remove the heat-shrinking tube and reopen the holes of each cannula in the array that resulted in clogging by cutting them by abrasion using a Dremel. With the help of a thin needle (i.e., 32G), deburr each opening to make it smooth and free of debris as well as clean inside each cannula using a stainless steel 34G bar.

2.4 Tetrode Twisting

Cut two pieces of your selected wire 20 cm long and align them together by one end of each thread. Bent the couple of wires on the middle keeping all tips together and making a loop around the horizontal main shaft of a tetrode spinning holder (Fig. 1c). Leave the free tetrode tips facing down of a custom tetrode twisting. Alternatively, if you do not have a spinning tetrode tool, it is possible to use any hot plate stirrer with a rotary magnet on its base (Fig. 1c). When this is the case, a metallic binder clip or metal hinge clip must be hanged from the free tips just on the opposite end to the loop (Fig. 1c). The distance between the clamp and the surface of the stir plate should be ~1.5 cm. This way, the rotary magnet under the surface of the steering plate will spin the metallic binder clip, and the four wires that compose a tetrode will spin too. Immediately after the binder clip and four wires start spinning, count approximately 90 full turns clockwise if working with NiCr wire. When the total number of turns is reached, stop the spinning tool or steering plate and allow the relaxation of the twisted wires, either by allowing it to spin in the opposite direction—this is approximately 30 turns when working with a tetrode twister—or by allowing the metallic binder to spin anti-clockwise until it stops by itself. Finally, use a heat gun to activate the wire coating that allows to fix and keep the characteristic twisted shape of a tetrode when it is removed from the horizontal bar where it was hanging over the spinner. Be careful not to apply excessive or moderate heat for too long or at a to short distance, which could melt the wire insulation, causing a short-circuit between the four channels of a tetrode. Move the heat gun up and down around the tetrode at medium temperature and a distance of 5 cm approx. The total number of spins will depend on the wire length, the type of alloy, and how much twist does the tetrode need. Also, some researchers would prefer to lightly modify the order of the steps, for instance, when a twisted tied tetrode is aimed, the heat can be applied before anticlockwise spinning the braided tetrode.

2.5 Electrode Interfacing Using a Custom-Printed Circuit Board

Using Altium Designer 2014, a custom double layer PCB was designed as the interface between electrodes and the headstage pre-amplifier. This PCB is built based on a standard FR-4 fiber glass of 600 μm of thickness, 1 Oz of copper, ENEPIG finish surface, and a green, yellow, or any other color available for the solder mask. On this PCB there are plated vias of 330 μm of diameter and an annular ring of 100 μm thick in both sides to improve the electric connection between the wire placed inside the via and the gold pin. Thirty-two vias are for the eight tetrodes, and the remaining vias are for the three ground connections and one for a reference channel. Typically, the ground wire consists of a perfluoroalkoxy alkane (PFA)-coated stainless steel, 0.003" bare, soldered to a 00–90 short stainless steel screw implanted in the skull touching the dura but without penetrating it. A military-grade connector (Omnetics Connector Corporation, model A79022-001) was soldered to this PCB using standard low-temperature solder paste (CHIPQUIK, SMDLTLFPT5) in a custom DIY reflow oven based on a commercial controller (i.e., Reflowster or Reflow Master). Alternatively, it is possible to use lead-free tin wire resin core and a soldering iron to hook the connector to the PCB by hand under the magnifier, although this approach is slower than the reflow soldering. If soldering by hand is still preferred, get help by using any tape, although polyimide is preferred given its thermal stability, or by using a cross-lock tweezer to hold the connector close to the PCB and proceed to soldering it. It is advised to cover the connector holes with tape to prevent to molten tin drops in the holes accidentally blocking them. After soldering, run a visual inspection to check if there are no shorts between the pins of the connector or shorts between PCB pads. With the help of a multimeter, check the proper continuity between each via and the corresponding connector pin. An overview of the connector attached to a PCB is shown in Fig. 1c.

3 Electrode Manipulator Assembly

3.1 Installing Cannulae Array Guide

First step is to mount the cannula array using cyanoacrylate and then dental acrylic in the center of the manipulator floor (Figs. 1a, d, 2a, b). After dental acrylic has thoroughly dried, separate the cannulae soldered free end (Fig. 2b), from the other cannulae to facility the interface with the 32G stainless-steel tubes (Fig. 2c). Before gluing the 32G cannulae to the movable system, turn the screw to rise the movable holder to the higher position. That will define the maximum distance that the tetrodes could be lowered (Fig. 2c). Glue the 32G to the holder using dental acrylic (Fig. 2d). Finally, slide each tetrode into the respective 32G tube of the eight cannulae array and glue each tetrode to the top portion of its respective 32G cannula using cyanoacrylate glue (Fig. 2d).

3.2 Interfacing Each Single Wire of a Tetrode with PCB

Once the electrode array is glued to the holder (Fig. 2d–f), it is time to proceed with the electrical contact between the wires and the PCB vias as mentioned above. For that, pass each wire of a tetrode through each corresponding via in the PCB (Fig. 2e). Write down to which set of vias (four vias per set) is each tetrode connected. It is preferable to pick them in a predetermined order according to a standard map used by your laboratory. This map must contain wires linking PCB vias information as well as identifying which electrode corresponds to which channel in the connector. This step ensures to associate the recorded signals to the targeted brain areas. After passing each wire per via, use small gold pins to make a strong electrical connection between the metal bar of each wire and the gold-plated wall and annular ring of a via. Finally, organize the wires around the connector (Fig. 2f) allowing free access to the holes on the top of the connector. Then fix the PCB to the microdrive by tightening the lateral screws and secure the PCB to the main body of the manipulator using dental cement (Fig. 2f).

3.3 Gold Plating

As mentioned before, the relationship between the surface area of the electrode tip, its impedance, and the signal-to-noise ratio is well known. Using a NiCr wire with a diameter between 12 and 17 μm, the impedance is over 3 MOhm when tested at 1 KHz before plating. For this reason and to reduce the wire impedance, each tetrode tip wire must be gold plated. A bigger signal-to-noise ratio will maximize the ability to record and discriminate action potentials sourced by single units. To achieve this, spin counterclockwise the screw of the microdrive system to put out from each guide tubing the tetrodes. Then, securely mount the microdrive on a clamp that will allow to submerge the wire tips into the gold plating solution. Fill an Eppendorf tube with a gold solution (i.e., Neuralynx™) and other with distilled water. Proceed to place the electrode tips in into the gold solution. We usually apply a DC current of 1.0 μA to each channel aiming to set the wire impedance around 250–350 kΩ using an isolated stimulator. If there is any single channel that has not been plated below 350 kΩ, repeat the process. Once all the tip wires have been gold plated, so the impedance is in an acceptable range, remove the electrode array from the gold plating solution and lower the tip of the tetrode array into distilled water to rinse off the excess gold particles. After rinsing the tetrode tips with water, it is convenient to use 70% alcohol and 100% alcohol as a final step. These two extra steps associated with the use of alcohol will help to keep the tetrode tips clean and remove the distilled water and moisture.

When gold plating and cleaning are done, pull up the electrode array to their top position leaving the tips immediately inside the guiding cannula. To do this, turn clockwise the drive screw. Thus, the microdrive and electrodes are ready for implantation.

3.4 Improving Signal-to-Noise Ratio

It is possible to use a tiny faraday cage inside a custom manipulator to electromagnetically insulate the electrodes and PCB from external electromagnetic interference or noise coming, for instance, from the alternating current (50 or 60 Hz depending on the country) associated with the power line. The main idea is to avoid that extra noise to interact with the metal portion of the implant such as electrodes and PCB that can work as antennas and translate such noise into currents that contaminate the action and field potentials recorded from the alive brain. Thus, the goal is to protect the electric neural signals just before they are amplified at the headstage level; leading to amplifications of biological signals with less electromagnetic interference. For this purpose, the manipulator can be covered on its internal wall with copper tape or copper mesh that is easily found in some hardware stores or online. After installing the Faraday cage shield, it has to be electrically connected to the ground at the PCB level. To achive this, a wire is glued to the internal wall of the manipulator using a copper tape or mesh, and connected to the other end of the ground PBC by a mechanical connection such as a gold pin or by soldering the wire directly into the PCB via.

4 Electrophysiological Setup

We built an amplification system combining custom software and commercial hardware. Thus, the amplification stages pertain to one commercial brand, while the analog to digital converter was acquired from a second-party hardware developer. The custom set of amplification and digitizing systems were interfaced with a Windows PC (Windows 10 Pro) where a custom-made software was wrote for data acquisition, spike extraction, and spike sorting.

Using the manipulator showed in the previous section, SNc recordings were performed using a 32-channel headstage (μPA 32, Multi Channel Systems) that allows a 10× pre-amplification of the signal. Then, the signals were amplified again (500×) on a second stage by a 32-channel amplifier (PGA 32, Multi Channel Systems) and band-pass filtered (1–5000 Hz). These data were sent to a USB National Instruments analog to digital converter (NI USB-6363, National Instruments), connected to a PC running a custom-made software written by Dr. Pedro Maldonado at the Universidad of Chile, Santiago, Chile. This software named "Get Data" was written on C with the help of LabWindows/CVI (National Instruments Inc.; version 10.0.0 (360), 2010) employing advanced signal analysis libraries (version 17.0, 2017). This custom software allows the offline visualization of each tetrode channel and then the storage of the digitized neural activity with a maximal temporal resolution of 30 KHz and a voltage precision of 16 bits. In this regard, when neural data was sampled at 30 kHz, this allows 32 data points for 1.07 ms time window to represent

each action potential waveform. Extracellular waveforms that exceeded a voltage threshold of two standard deviations from the average noise were extracted. The action potential waveforms were extracted and represented by 32 voltage data points, having 10 data points to the voltage value data points pre-threshold and 22 data points for the post-threshold.

For our following data, two adult male Sprague Dawley rats were used. All procedures were in strict accordance with the guidelines published in the "NIH Guide for the Care and Use of Laboratory Animal" (8th Edition) and the principles presented in the "Guidelines for the Use of Animals in Neuroscience Research" by the Society for Neuroscience. When we recorded neural electric activity on rodents under anesthesia, we use urethane (1.5 g/kg i.p) since it does not modify normal firing patterns of DA neurons [24, 25]. The rat was then positioned in a stereotaxic apparatus (Stoelting Co). A craniotomy on the following coordinates was performed, relative to bregma: anteroposterior = −4.8 to −5.2 mm, mediolateral = −3.0 to −2.0 mm. The size of the craniotomy must be wide enough to position the tube array that is ~1.2 mm × 0.7 mm. After removing the dura mater, lower the tube array until it touches the brain, without perforating it. It is a good practice to use some type of sealing such as agar around the cannulae array to protect the brain underneath. To lower the tetrodes, use the screw from the microdrive. Tetrodes are first lowered at a 312 μm every 10 s rate (one full turn of the screw), until reaching the beginning of the targeted region. SNc is located in the following coordinates: dorsoventral = −7.6 to −8.0 mm. To search for single units, lower the tetrodes at a ~38 μm rate (1/8 turn of screw). If it is possible, try to find single unit activity in all the tetrodes (or at least in a half of them) and then wait 30–45 min until the single unit activity seems to be stable. More details about single unit identification and extraction are described on the following section.

5 Qualitative and Quantitative Analysis of the Discharge Pattern of SNc Neurons

Changes on the rate (spikes/second) and mode of discharging action potentials (i.e., bursty versus a tonic pattern) of neurons in response to amphetamine (AMPH) and other psychostimulants have been reported. In this regard, preclinical studies have shown consistent evidence of neuroplastic changes in the mPFC [26] and the dorsolateral striatum (DLS) [20, 21] induced by AMPH and cocaine [27]. However, the data regarding the effect of AMPH on SNc neurons is sparse, and the preliminary data we show in this chapter might contribute to fill the gap. In this regard, we discussed quantitative and qualitative changes on the firing rate of putative DA neurons recorded from the SNc on anesthetized rats after an acute AMPH injection.

Using "Get Data" software, it is possible to visualize the raw signal of the four channels of a tetrode in an offline mode as in the Fig. 3a. It is possible to see how the amplitude of the spikes pertaining to a neuron is different among channels at the same time point; however, the noise event shows up simultaneously with the same amplitude in all the four channels of a tetrode. The spike extraction was made on "Get data," while the clustering was made with the help of the software "Spike Sorter" also wrote by Dr. Pedro Maldonado (1999) using LabWindows/CVI. In both cases we used the Windows version of such software. Waveforms were sorted mainly using two-dimensional plots of the peak-to-peak amplitude of action potentials for pairs of two channels from the same tetrode (Fig. 3b). Also, it is possible to use principal component analysis of the spike waveforms to confirm the clustering defined on the scatter plots. Basically, we searched through different combinations of the channels pertaining to the same tetrode where the clusters did not overlap. Isolated clusters were used to obtain the average waveforms $\pm$ standard deviation based on all the spikes in a cluster pertaining to each single units recorded (Fig. 3d). Additionally, each timestamp associated with each spike when neurons discharge action potentials was extracted (Fig. 3c). Using the timestamps, we computed standard analytics per neurons described on the coming sections. As depicted on Fig. 3f and discussed on some of the early seminal works, (i) the electric distance from voltage membrane to electrode tip, (ii) the relative position of electrode tip in relationship to the neural body, and (iii) the surface area of electrode tip [15, 16], as well as (iv) the spatial relationship among channels that are part of an tetrode [28, 29], determine the spatial resolution and waveforms of the recorded action potentials. Also, it is important to note that when the extracellular recordings involve cells with a wide waveform as neuron 1 depicted on Fig. 3d, further analysis can be optimized by increasing the time window and ideally the number of samples for such time windows, to capture the whole action potential and details of waveform, respectively. For DA neurons, a time window of 1.4 ms has been used previously in tetrode recordings [30].

Following spike sorting, we proceeded with the analysis of firing parameters of SNc neurons. Here we analyzed the firing rate and firing pattern measures such as the interspike interval (ISI), autocorrelograms, and their respective power spectrums. Neurons with a percentage of ISI < 2 ms greater than 1% were considered as multi-units and excluded for further analysis to avoid false positives about firing patterns. Twenty-one neurons were finally used in the analytics discussed in this chapter.

A representative data analysis for single units is showed in Fig. 4, using two neurons from our data of SNc single-cell recordings (red and black trace in Fig. 4c–f). The main data needed to proceed to single-unit analysis is the timestamp or its respective binary file with a 1 ms time resolution. To obtain the spike

timestamp associated with each single cell, the digitized signal (Fig. 4a, top) was analyzed by a clustering procedure shown in Fig. 3b–d. The time when each of these spikes was found was consolidated in a timestamp file (Fig. 4b, top; a raster plot was created from the timestamps depicted on the bottom). Finally, the timestamp file can be transformed to a binary file (Fig. 4b, bottom). The binary file is a continuous series of zeros and ones (in a millisecond scale), which allows to identify the occurrence of a spike in a logical (true or false) matter: a one represents that a spike is found in that millisecond, whereas a zero show the absence of a spike.

In our current experiments, we used the following recording protocol to study the effect of an acute AMPH injection: 10 min of basal activity, 20 min of post-saline injection, and 30 min of post-AMPH 1.0 mg/kg injection. Figure 4c shows the time course of firing rate during the 60 min of recording from two SNc neurons (bin size = 1 min). Firing rate was calculated dividing the total number of spikes in a period divided by the total time of that period. Then, data was plotted as a *Z*-score, to better visualized how the firing rate deviate from the basal in response to AMPH. This *Z*-score can be obtained as follows:

$$\frac{X \text{ firing rate} - \text{mean baseline firing rate}}{\text{standard deviation baseline firing rate}}$$

where X is the firing rate on a specific time, in this case for a bin size of 1 min. The *Z*-score vs time plot showed a sustained increment (*Z*-score > 2) on firing rate of the red trace neuron but not in the firing rate of the neuron depicted by the black trace. While *Z*-score can be used to study the statistical significance of the firing rate changes after a stimulus such as AMPH or lithium chloride, we recommend using a more robust statistical method like the non-parametric permutation test [21, 22]. First, baseline and post-AMPH firing rate of an individual neuron were divided in 1-min bins. Then, the mean firing rate of the baseline and post-AMPH bins was calculated, and the difference between them (original mean) was computed. Then, to estimate the empirical distribution of the test statistic under the null hypothesis, we randomly mixed the binned firing rate of baseline and post-AMPH and then computed the difference of the mean firing rate in the same manner (new mean firing rate). This permutation process was repeated 1000 times, and a distribution using all the new means firing rate differences was obtained. Finally, by comparing the test statistic computed using the original mean to the estimated empirical distribution, we calculated the p value and rejected the null hypothesis when the probability associated with test statistic was less than a significance level of 0.05. Using this method, the red trace neuron was classified as an excited neuron to AMPH (i.e., the neuron increased its firing rate after AMPH injection) and the neuron represented by the trace in black as neuron that did not change its firing rate in response to AMPH.

The firing pattern of a neuron can be visualized using ISI histograms (Fig. 4d). The ISI is defined as the difference in time between adjacent spikes fired by a single cell. It is computed with the timestamp data file (or transforming the binary file to timestamp). Following, this data is plotted in histograms, with the number of counts in each bin of time and normalized by the total number of ISIs (spike probability). The red and black trace neurons showed a similar ISI histogram during baseline and post-saline injection, indicating that their firing pattern did not change during these periods. During post-AMPH, a change in the ISI histogram distribution was found in the black trace neurons, showing a higher spike probability than the red trace neuron between 80 and 100 ms. This suggest a change in firing mode of the black trace neurons after AMPH injection that was not accompanied by a modification in firing rate. It is important to note that the total amount of spikes ($N = 3700$) was the same for each histogram.

A complementary analysis for firing pattern is the autocorrelogram. It is defined as the correlation of a spike train with itself but with a lag. Normalized autocorrelogram was calculated using the binary file as input for the *xcorr* MATLAB function using the following parameters: maxlag = 1024 (range of ± 1024 ms) and scaleopt = "coeff" (this specifies normalization). This function calculates the normalized correlation between the binary data and the binary data with a lag (lag = 0 is omitted, because it is always 1). Autocorrelogram curves were smoothed using a 25 ms hamming window (MATLAB; *filter* function). As in ISI analysis, our results showed similar autocorrelogram curves for the two neurons during baseline and post-saline (Fig. 4e). The lower probability values in the red trace neurons around 100 ms are because these neurons showed longer lag times between spikes. Importantly, during post-AMPH, the black trace neuron shows an increment in the normalized number of spikes between 80 and 100 ms as observed in Fig. 4d3. This confirms that a specific pattern of neuronal activity emerges in response to AMPH as depicted for the black trace neuron.

Last, the oscillatory nature of the autocorrelogram can be analyzed using a fast Fourier transform (MATLAB; *fft* function). Plotting the spectrum of amplitude vs frequency, it is possible to find the characteristic frequency at which the recorded SNc neurons respond to AMPH. In our example results, we found that the main difference between neurons was around 11 Hz of oscillatory activity after AMPH injection (Fig. 4f). The black trace neuron shows an increase between 9 and 14 Hz in response to AMPH (gray shade area), a result that is expected considering the data found in the ISI and autocorrelograms, where the spike firing was more evident within 80–100 ms. Overall, these analyses allow a fine dissection of the firing signatures of a neuron in response to drug administration.

6 Classification of Dopaminergic Neurons and Effect of an AMPH Injection

The activity of DA neurons has been widely studied (for review, *see* ref. 31). Many of the studies in DA neurons have been performed using glass pipettes [32–34] that are optimal to record single units but have a disadvantage: only one cell at a time is recorded per pipette. In this sense, the use of tetrodes has the advantage that with one single tetrode, several single units can be recorded (as showed in Fig. 3). However, we must consider that around the SNc, not only DA neurons are found but also GABAergic neurons and interneurons (for review, *see* ref. 35), evidencing the need to use several electrophysiological parameters to differentiate DA neurons. In electrophysiological recordings using pipettes, the following parameters were defined to classify a neuron as dopaminergic: (i) recording location; (ii) action potential duration >2.2 ms (unfiltered), >1.1 ms (filtered; 300–5000 Hz); (iii) firing rate <10 Hz; and (iv) bursty firing pattern, with a burst episode starting with an ISI < 80 ms and burst ending when ISI > 180 ms [36]. Here in this chapter, we explore the classification of DA neurons based on extracellular recordings using tetrodes.

For the analysis of phenotypes to identify putative DA neurons, we adapted some parameters that allowed us to classify striatal medium spiny neurons from anesthetized [20] and freely moving [21] recordings. The classification protocol we used considers the spike waveform and timestamp analyses (firing rate and ISI) of each neuron. First, each averaged waveform was normalized by their peak amplitude value and plotted for each of the 21 neurons (Fig. 5a) analyzed in this chapter. Differences on the waveforms after the peak were found among three potential clusters. This measure here is called repolarization at 0.3 ms (vertical black dotted line in Fig. 5a; [37]). To divide the waveforms in different subpopulations, we can combine the repolarization at 0.3 ms, for instance, with the peak-to-amplitude ratio (PAR, [38]) that is defined as follows: peak value/peak to valley value. Figure 5b shows a scatter plot of PAR vs repolarization at 0.3 ms for the 21 SNc neurons analyzed in this chapter. To obtain the clusters of neurons based on the repolarization vs PAR data, the MATLAB *kmeans* function was used. Three clusters were obtained. As defined before, the action potential duration of DA neurons is higher than 1.1 ms in filtered signals like in tetrodes [36]. In this sense, neurons from the second (red) and third (green) clusters were candidates to be defined as putative DA neurons, as they show large action potential durations. Given the sharp and more symmetric action potential waveform, neurons from the first cluster depicted in blue (Fig. 5a) could be considered as a population of putative GABAergic neurons [35].

To confirm which of the two clusters showing large action potential correspond to the DA neurons, firing parameters were also analyzed. In this regard, the ISI histograms were obtained from each neuron and then plotted as the averaged ISI for each one of the three clusters (Fig. 5c, time in logarithmic scale to show large ISI values) vs spike probability. The first (blue) and third (green) clusters showed a similar distribution of their ISI values, with a large proportion of their being higher than 1 s (10^0 s). Interestingly, the ISI distribution of the second cluster depicted in red (Fig. 5c) showed a peak around 0.1 s (10^{-1} s). To analyze if the ISI histograms were significantly different between clusters, we obtained the skewness value of the ISI distributions (MATLAB; *skewness* function). Based on extracellular tetrode recordings, it has been previously defined that DA neurons show an ISI skewness value around 2 [39, 40]. Indeed, the second neural cluster depicted in red shows a skewness median value around 2. This means the cluster of putative DA neurons shows a biased distribution to short ISI, whereas skewness values close to 0 show a uniform distribution. Moreover, the proportion of ISIs higher than 2 s (number of ISIs >2 s/total number of ISIs) was the lowest for the cluster of putative DA neurons and more uniform for the first and third clusters (Fig. 5e). Thus, these results strongly suggest that the second cluster depicted in red corresponds to a set of DA neurons recorded from the SNc (Fig. 3e). The ISI histogram and ISI skewness reported here are similar to those previously described for DA neurons [34, 39, 40]. While it is not clear to which neuronal phenotype the neurons from the third cluster could correspond, even considering the long waveform and irregular firing pattern, it is safer to leave these neurons as an unidentified phenotype.

When looking to more common parameters as the basal firing rate (Fig. 5f), we also observed that the cluster of putative DA neurons showed a median activity of 8 Hz as reported for DA neurons [31].

Burst activity has been commonly analyzed on DA neurons using the following criteria [34]: a burst begins when two spikes are found within 80 ms and ends when an ISI larger than 160 ms is observed. Also, the coefficient of variation (defined as the standard deviation of the ISI divided by the mean of the ISIs) has been used for the same purpose [24]. However, this method has the caveat that is dependent on the firing rate. To address this and to avoid using an arbitrary threshold as the Grace and Bunney method [34], we measured the local variation index (Lv). This is an index about firing mode and was calculated as follows [41]:

$$\mathrm{Lv} = \frac{3}{n-1} \sum_{i=1}^{n-1} \left(\frac{I_i - I_{i+1}}{I_i + I_{i+1}} \right)^2$$

where I_i and I_{i+1} correspond to the i-th and i + 1st ISIs and n are the number of ISIs. Then, Lv index allows to analyze the instantaneous variability of ISIs, with the advantage that this index is less sensitive to changes on firing rate compared to the coefficient of variation. Thus, Lv range from values under to around one (1) means a regular to irregular pattern, respectively, while values over 1 point to a firing mode type burst. For our current data, we found that the cluster of putative DA neurons showed a lower Lv than the other two clusters ($p < 0.05$, Mann-Whitney test, Fig. 5g). This result is consistent with that reported in the literature for DA neurons with a regular firing rate [24].

In summary, based on extracellular tetrode recordings, single cells can be defined as putative DA neurons if they meet the following criteria based on the data discussed so far:

- PAR between 0.8 and 0.95 (Y-axis, Fig. 5b)
- Repolarization at 0.3 ms between −0.13 and 0 ms (X-axis, Fig. 5b)
- Median skewness around 2 (Y-axis, Fig. 5d)
- High % of low chance of ISIs >2 s (Y-axis, Fig. 5e)
- Basal firing rate ~8 Hz (Y-axis, Fig. 5f)
- Basal Lv ~0.5 (Y-axis, Fig. 5g)

After attempting the classification of SNc cells as DA neurons based on the criteria described above, then we studied the effect of an acute AMPH 1.0 mg/kg ip injection on the sample of SNc neurons (Fig. 6). We found that an acute AMPH injection induced an increment on the firing rate (Fig. 6a, cluster 2, $p < 0.05$, Wilcoxon signed-rank test) of all the five putative SNc DA neurons (Fig. 6c, cluster 2, $p < 0.05$, permutation test). The putative GABAergic neurons in the first cluster were also mainly excited in response to AMPH, while the unidentified third cluster of neurons showed a mixed response to AMPH. Putative DA neurons did not show a change on their firing pattern in response to AMPH ($p > 0.05$, Wilcoxon signed-rank test, Fig. 6b), while putative GABAergic neurons adjust their firing in response to AMPH. Overall, these results indicate that putative SNc DA neurons are mainly excited by AMPH but did change their firing pattern. Also, we only record a small number of neurons with five putative SNc DA neurons that constitute a very preliminary result.

Remarks

In this chapter, we discussed the extraction of waveform and firing parameters to characterize putative neural phenotypes from the recording of single unit on anesthetized rats. The flexibility of this method makes it possible to use exactly the same analyses on free-behaving animals, altogether with pharmacological and

optogenetic manipulations to increase robustness, and more importantly to explore causal hypothesis about the contribution of different neural phenotypes to physiological and behavioral disorders. Thus, it should be possible to better understand how the neural signature evolves in correlation with the casual drug intake to habits. It is well known that the behavioral sensitization by AMPH is a good approach to better understand the evolution of drug addiction. In this regard, we started using the Lv index on medium spiny neurons activity recorded from the dorsolateral striatum of anesthetized [20] and freely moving rats [21]. In these studies we found a higher Lv, meaning that a burst firing pattern predicted the susceptibility to express AMPH locomotor sensitization. Then, after a repeated AMPH administration, a challenge of this psychostimulant on sensitized rats was associated with a decrease in the Lv index. Dorsolateral striatum neurons showed a regular tonic likewise firing pattern in response to AMPH [21]. This experimental approach can be extended to the recording of multiple sites, for instance, from where DA neurons are placed to the brain areas targeted by their projections.

The scope of our approach is electrode agnostic. Given that the main parameters used to identify different neural phenotypes are the spike waveform and their timing, our approach is valid for intra- and extracellular recordings, while the minimum condition of capturing the action potential waveforms and timestamps from single units is achieved. Importantly, we also here described an easy and versatile electrode array configuration that allows such goal based on basic laboratory tools and materials. In this regard, the custom microdrive described in this chapter is a cheap and very accessible solution for electrophysiological recordings on anesthetized or freely moving animals. The main advantage of such a physical platform is its flexibility to control electrode positioning of multiple electrode bundles that are part of the same manipulator and can target several brain areas simultaneously.

Bibliography

1. Cools R (2008) Role of dopamine in the motivational and cognitive control of behavior. Neuroscientist 14(4):381–395
2. Robbins TW, Gillan CM, Smith DG, de Wit S, Ersche KD (2012) Neurocognitive endophenotypes of impulsivity and compulsivity: towards dimensional psychiatry. Trends Cogn Sci 16(1):81–91. https://doi.org/10.1016/j.tics.2011.11.009
3. Escobar AP, Casanova JP, Andrés ME, Fuentealba JA (2020) Crosstalk between kappa opioid and dopamine systems in compulsive behaviors. Front Pharmacol 11:57. https://doi.org/10.3389/fphar.2020.00057. eCollection 2020. Review
4. Fallon JH, Moore RY (1978) Catecholamine innervation of the basal forebrain. IV. Topography of the dopamine projection to the basal forebrain and neostriatum. J Comp Neurol 180:545–580
5. Fallon JH, Riley JN, Moore RY (1978) Substantia nigra dopamine neurons: separate populations project to neostriatum and allocortex. Neurosci Lett 7:157–162

6. Haber SN, Fudge JL, McFarland NR (2000) Striatonigrostriatal pathways in primates form an ascending spiral from the shell to the dorsolateral striatum. J Neurosci 20(6):2369–2382. https://doi.org/10.1523/JNEUROSCI.20-06-02369.2000
7. Pérez-Valenzuela EJ, Andrés Coke ME, Grace AA, Fuentealba Evans JA (2020) Adolescent exposure to WIN 55212-2 render the nigrostriatal dopaminergic pathway activated during adulthood. Int J Neuropsychopharmacol 23(9):626–637. https://doi.org/10.1093/ijnp/pyaa053
8. Marinelli M, Cooper DC, Baker LK, White FJ (2003) Impulse activity of midbrain dopamine neurons modulates drug-seeking behavior. Psychopharmacology 168(1–2):84–98. https://doi.org/10.1007/s00213-003-1491-1
9. Buzsáki G, Costas AA, Christof K (2012) The origin of extracellular fields and currents—EEG, ECoG, LFP and spikes. Nat Rev Neurosci 13(6):407–420. https://doi.org/10.1038/nrn3241
10. della Valle E, Koo B, Patel PR, Whitsitt Q, Purcell EK, Chestek CA, Weiland JD (2021) Electrodeposited platinum iridium enables microstimulation with carbon fiber electrodes. Front Nanotechnol 3:782883. https://doi.org/10.3389/fnano.2021.782883
11. Paxinos G, Charles W (2007) The rat brain in stereotaxic coordinates, 6th edn. Elsevier
12. Swanson LW (2004) Brain maps: structure of the rat brain, 3rd edn. Elsevier
13. Jo YS, Heymann G, Zweifel LS (2018) Dopamine neurons reflect the uncertainty in fear generalization. Neuron 100(4):916–925.e3. https://doi.org/10.1016/j.neuron.2018.09.028
14. Heymann G, Jo YS, Reichard KL, McFarland N, Chavkin C, Palmiter RD, Soden ME, Zweifel LS (2020) Synergy of distinct dopamine projection populations in behavioral reinforcement. Neuron 105(5):909–920.e5. https://doi.org/10.1016/j.neuron.2019.11.024
15. Robinson DA (1968) The electrical properties of metal microelectrodes. Proc IEEE 56(6):1065–1071. https://doi.org/10.1109/PROC.1968.6458
16. Lemon R (1984) Methods for neuronal recording in conscious animals. Wiley
17. Buzsáki G (2004) Large-scale recording of neuronal ensembles. Nat Neurosci 7(5):446–451. https://doi.org/10.1038/nn1233
18. Kaltenbach JA, Gerstein GL (1986) A rapid method for production of sharp tips on preinsulated microwires. J Neurosci Methods 16(4):283–288. https://doi.org/10.1016/0165-0270(86)90053-1
19. Olds J, Disterhoft JF, Segal M, Kornblith CL, Hirsh R (1972) Learning centers of rat brain mapped by measuring latencies of conditioned unit responses. J Neurophysiol 35(2):202–219. https://doi.org/10.1152/jn.1972.35.2.202
20. Gatica RI, Aguilar-Rivera MÍ, Azocar VH, Fuentealba JA (2020) Individual differences in amphetamine locomotor sensitization are accompanied with changes in dopamine release and firing pattern in the dorsolateral striatum of rats. Neuroscience 427:116–126. https://doi.org/10.1016/j.neuroscience.2019.11.048
21. Gatica RI, Aguilar-Rivera M, Henny P, Fuentealba JA (2022) Susceptibility to express amphetamine locomotor sensitization correlates with dorsolateral striatum bursting activity and GABAergic synapses in the globus pallidus. Brain Res Bull 179:83–96. https://doi.org/10.1016/j.brainresbull.2021.12.005
22. Aguilar-Rivera M, Kim S, Coleman TP, Maldonado PE, Torrealba F (2020) Interoceptive insular cortex participates in sensory processing of gastrointestinal malaise and associated behaviors. Sci Rep 10(1):21642. https://doi.org/10.1038/s41598-020-78200-w
23. Manzur HE, Alvarez J, Babul C, Maldonado PE (2013) Synchronization across sensory cortical areas by electrical microstimulation is sufficient for behavioral discrimination. Cereb Cortex 23(12):2976–2986. https://doi.org/10.1093/cercor/bhs288
24. Brown MT, Henny P, Bolam JP, Magill PJ (2009) Activity of neurochemically heterogeneous dopaminergic neurons in the substantia nigra during spontaneous and driven changes in brain state. J Neurosci 29(9):2915–2925. https://doi.org/10.1523/JNEUROSCI.4423-08.2009. PMID: 19261887; PMCID: PMC4262786
25. Walczak M, Błasiak T (2017) Midbrain dopaminergic neuron activity across alternating brain states of urethane anaesthetized rat. Eur J Neurosci 45(8):1068–1077. https://doi.org/10.1111/ejn.13533
26. Aguilar-Rivera MI, Casanova JP, Gatica RI, Quirk GJ, Fuentealba JA (2015) Amphetamine sensitization is accompanied by an increase in prelimbic cortex activity. Neuroscience 288:1–9. https://doi.org/10.1016/j.neuroscience.2014.12.027
27. Steketee JD, Kalivas PW (2011) Drug wanting: behavioral sensitization and relapse to drug-seeking behavior. Pharmacol Rev 63(2):

348–365. https://doi.org/10.1124/pr.109.001933

28. Gray CM, Maldonado PE, Wilson M, McNaughton B (1995) Tetrodes markedly improve the reliability and yield of multiple single-unit isolation from multi-unit recordings in cat striate cortex. J Neurosci Methods 63(1–2):43–54. https://doi.org/10.1016/0165-0270(95)00085-2
29. Harris KD, Henze DA, Csicsvari J, Hirase H, Buzsáki G (2000) Accuracy of tetrode spike separation as determined by simultaneous intracellular and extracellular measurements. J Neurophysiol 84(1):401–414. https://doi.org/10.1152/jn.2000.84.1.401
30. Wang DV, Tsien JZ (2011) Conjunctive processing of locomotor signals by the ventral tegmental area neuronal population. PLoS One 6(1):e16528. https://doi.org/10.1371/journal.pone.0016528. PMID: 21304590; PMCID: PMC3029369
31. Marinelli M, McCutcheon JE (2014) Heterogeneity of dopamine neuron activity across traits and states. Neuroscience 282:176–197. https://doi.org/10.1016/j.neuroscience.2014.07.034
32. Grace AA, Bunney BS (1983) Intracellular and extracellular electrophysiology of nigral dopaminergic neurons--1. Identification and characterization. Neuroscience 10(2):301–315. https://doi.org/10.1016/0306-4522(83)90135-5. PMID: 6633863
33. Grace AA, Bunney BS (1984) The control of firing pattern in nigral dopamine neurons: single spike firing. J Neurosci 4(11):2866–2876. https://doi.org/10.1523/JNEUROSCI.04-11-02866.1984
34. Grace AA, Bunney BS (1984) The control of firing pattern in nigral dopamine neurons: burst firing. J Neurosci 4(11):2877–2890. https://doi.org/10.1523/JNEUROSCI.04-11-02877.1984
35. Dudman JT, Gerfen CR (2015) Chapter 17 – The basal ganglia. In: Paxinos, George. Academic Press, San Diego, pp 391–440
36. Ungless MA, Grace AA (2012) Are you or aren't you? Challenges associated with physiologically identifying dopamine neurons. Trends Neurosci 35(7):422–430. https://doi.org/10.1016/j.tins.2012.02.003
37. Vinck M, Bos JJ, Van Mourik-Donga LA, Oplaat KT, Klein GA, Jackson JC, Gentet LJ, Pennartz CMA (2016) Cell-type and state-dependent synchronization among rodent somatosensory, visual, perirhinal cortex, and hippocampus CA1. Front Syst Neurosci 9:1–25. https://doi.org/10.3389/fnsys.2015.00187
38. Yarom O, Cohen D (2011) Putative cholinergic interneurons in the ventral and dorsal regions of the striatum have distinct roles in a two choice alternative association task. Front Syst Neurosci 5:5–36. https://doi.org/10.3389/fnsys.2011.00036
39. Li W, Doyon WM, Dani JA (2011) Acute in vivo nicotine administration enhances synchrony among dopamine neurons. Biochem Pharmacol 82(8):977–983. https://doi.org/10.1016/j.bcp.2011.06.006. Epub 2011 Jun 12. PMID: 21684263; PMCID: PMC3162092
40. Doyon WM, Ostroumov A, Ontiveros T, Gonzales RA, Dani JA (2021) Ethanol produces multiple electrophysiological effects on ventral tegmental area neurons in freely moving rats. Addict Biol 26(2):e12899. https://doi.org/10.1111/adb.12899
41. Shinomoto S, Kim H, Shimokawa T, Matsuno N, Funahashi S, Shima K, Fujita I et al (2009) Relating neuronal firing patterns to functional differentiation of cerebral cortex. PLoS Comput Biol 5(7):e1000433. https://doi.org/10.1371/journal.pcbi.1000433